Reduction of natrojarosite and laterite nickel ore leaching residue composite using palm kernel shell reducing agents at temperatures of 1300-1450℃

Afif Nur Iksan[1] , *Zulfiadi* Zulhan[1], *Achmad* Haerul Yusro[2], and *Taufiq* Hidayat[1]

[1]Metallurgical Engineering Research Group, Faculty of Mining and Petroleum Engineering, Bandung Institute of Technology, Bandung 40132, Indonesia
[2]PT Hydrotech Metal Indonesia, Jl. Raya Narogong km 26, Klapanunggal, Bogor, 16710, Indonesia

Abstract. Lateritic nickel ore processing through hydrometallurgical route generates a significant amount of residue from the leaching stage. Two examples of hydrometallurgical process residues, namely natrojarosite and leaching residue can potentially be used as secondary raw materials for the iron and steel industry. A relatively high sulfur content of up to 12% is a severe issue because the sulfur threshold value for steel raw materials is 1%. Therefore, it is necessary to reduce the sulfur content in natrojarosite and leaching residue to meet the standards as a secondary raw material for the iron and steel industry. In this research, reduction of natrojarosite, laterite nickel ore leaching residue, and palm kernel shell reducing agents composite was conducted in varying amounts of palm kernel shell reductant of 25-100% using a non-isothermal method at an initial temperature of 1000ºC with a final temperature of 1300-1450ºC and an isothermal method of 1000ºC, 1300ºC, and 1450ºC for 2 hours. The results showed that an excessive amount of reductant (≥25%) would inhibit the formation of iron metal at macrosize (above 0.35 mm). Reduction, both by non-isothermal and isothermal methods, results in decreasing sulfur content in the metal phase as the reduction temperature increases, but a sulfur-rich matte phase is still observed in all experimental conditions. The proportion of the metal phase produced is getting higher and more separated from the slag phase as the temperature increases. The optimum condition was obtained at a non-isothermal reduction of 1450ºC using a 25% reducing agent which resulted in iron and sulfur content in the metal phase of 88.53% and 0.49%, respectively, with a metal-matte phase proportion of 65.56%. In this case, slag was dominated by liquid phase with a FeO content of 7.64% and a viscosity of 7.313 PaS.

1 INTRODUCTION

Development of stainless-steel industry, Li-ion battery industry, and nickel-based super alloy industry have implications for the increasing global demand for nickel. This provides an opportunity for Indonesia to utilize its significant nickel reserves which is the largest in the world in 2022, namely 21 million tonnes in the form of nickel laterite[1]. Prior to 2014, mining companies in Indonesia exported lateritic nickel ore massively, for instance limonite ore was exported to Australia, low grade saprolite was exported to China, and high grade saprolite was exported to Japan[2]. The 2009 Mining Law was introduced which requires nickel mining companies to process laterite nickel ore domestically starting on January 12, 2014.

Processing of lateritic nickel ore, especially the limonite type, is generally carried out through the hydrometallurgical route. One of the proven and existing nickel hydrometallurgical technologies in Indonesia is the High-Pressure Acid Leaching (HPAL) technology used by PT HPL on Obi Island, North Maluku. Apart from that, there is another technology that is being developed by PT HMI known as the Step - Temperature Acid Leaching (STAL) process. This process involves sulfatization, roasting with temperature intervention, and water leaching. This technology is considered to be able to significantly reduce sulfuric acid consumption at the leaching stage thereby contributing to reduced capital and operating costs as well as having high flexibility to process a variety of nickel ore deposits ranging from nickel limonite to saprolite types[3].

Nickel hydrometallurgical process has major problems related to the large amount of residual processing results from the leaching stage which has the potential to pollute the environment in the long term and needs to be managed according to hazardous waste handling procedures[4]. Based on data from the 2021 Ministry of Energy and Mineral Resources, the hydrometallurgical process, especially HPAL, produces residual waste reaching 128 tonnes per tonne of nickel, or around 3 times from the pyrometallurgical process through RKEF technology. There are 4 ways to handle the residual nickel processing, namely deep sea tailing placement (DSTP), backfilling, tailing dam disposal, and tailing reuse disposal[5,6]. Handling residual waste using the DSTP method is the cheapest and easiest option because of the short waste management duration, does not require large areas for placing waste on land,

and is suitable for factories located near ocean areas. But, after the enactment of Government Regulation No. 101 of 2014, tailings resulting from the smelting and refining process are classified as B3 waste, so it is prohibited to dispose of them by DSTP. Handling waste using this method can contaminate the marine ecosystem and the health of the surrounding community which accumulates through the food chain. Therefore, waste handling has switched to the dry tailing storage method. However, this method requires a large enough area for land storage and its nature will continue to be permanent if it is not utilized further. It also poses a risk to the surrounding environment in the event of heavy rainfall which may cause the waste to overflow from the storage area.

Natrojarosit is an example of the residue from nickel hydrometallurgical processing through STAL technology, which is a by-product of iron and aluminum precipitation from the leaching solution. In general, the iron content in jarosite reaches 20-35% with high sulfur levels[7]. In addition, other processing residue that is of major concern is leaching residue i.e. residual material from the leaching stages from which valuable minerals has been extracted. Leaching residue has an iron content of around 30-60%[8,9]. The large quantity of natrojarosite and leaching residue is a problem that needs to be addressed to minimize contamination and hazards to the environment and surrounding ecological systems[4,10,11]. Natrojarosit and leaching residue have great potential to be further utilized based on their valuable mineral contents. An alternative utilization of the residual results from this processing is by extracting the iron contained in it. The iron produced can be utilized as a secondary raw material for the manufacture of iron and steel.

This research focuses on the extraction of iron from a mixture of natrojarosite and laterite nickel ore leaching residue. The process involves direct reduction of varied amounts of reducing agents and at different reduction temperatures. The sulfur content in the reduced iron and the formation of sulfur-containing phase are investigated thoroughly. The slag produced is also examined to identify its characteristics on the difference in heating profile and temperature at the end of the reduction process. This research is expected to provide solutions to problems related to residual nickel hydrometallurgical processing where the reduced product can be used as a secondary raw material for the iron and steel industry.

2 MATERIALS AND METHODS

2.1 Materials

This research was carried out using natrojarosite and laterite nickel ore leaching residue supplied by PT Hydrotech Metal Indonesia. Results of the elemental analysis of natrojarosite and laterite nickel ore leaching residue are shown in Table 1 and 2 whereas the phase analyses are provided in Fig. 1 and 2. Natrojarosite contains calcium sulfate hydrate, natrojarosite, and bassanite as major phases, whilst laterite nickel ore leaching residue contains hematite, magnetite, and natrojarosite as major phases. Based on Table 1 and 2, the CaO content in natrojarosite is lower than the SiO_2 content. Conversely, the content of SiO_2 in laterite nickel ore leaching residue is significantly higher than the content of CaO. The amount of CaO and SiO_2 directly affects the basicity of the resulting slag. Too high or too low basicity is undesirable in the reduction process. Therefore, the present reduction test was performed using raw material in the form of natrojarosite and leaching residue composite since the mixture of both materials at specific proportion can optimize the composition of the slag so that there can be a good separation between the slag phase and the metal phase in the reduced sample. The reducing agent used was palm kernel shell with a fixed carbon of 18.60% as shown in Table 3.

2.2 Methods

Samples were prepared by drying at 130°C for 10 hours, crushing, grinding, and sieving to a size of 65 mesh. Whilst palm kernel shell reducing agent was pulverized to a grain size of 200 mesh. Then, sampling was carried out using the coning and quartering method to obtain a sample that represents the entire population. Initial characterization was conducted by X-ray Fluorescence (XRF, Rigaku ZSX Primus IV, Tokyo Japan), X-ray Powder Diffraction (XRD, Shimadzu XRD-7000 maxima, Kyoto, Japan), and proximate analysis. In addition, the reduced samples was also analyzed using a Scanning Electron Microscope – Energy Dispersive Spectroscopy (SEM-EDS, JEOL JCM 7000 NeoScope™, Tokyo, Japan).

Samples consisted of natrojarosite and leaching residue composite at a ratio of 20%:80% on a total basis of 2 grams. Then, the palm kernel shell reducing agent was also added at mass ratio to the natrojarosite–leaching residue composite of 25%, 50%, 75%, and 100%. The sample to be reduced was formed into composite briquettes at a pressure of 5 tonnes for 10 minutes. Briquette was put into an alumina crucible which was already filled with bed reductor and equipped with graphite lid. The reduction process was conducted in a calibrated muffle furnace (XINYO XD-1700M, Jiangsu, China). Reduction was carried out using 2 different methods i.e. non-isothermal and isothermal. Non-isothermal reduction was performed at an initial temperature of 1000°C with variations of final temperature of 1300°C, 1350°C, 1400°C and 1450°C. The crucible was placed into the muffle furnace at a temperature of 1000°C and was held isothermally for 30 minutes then the temperature was raised at a rate of 7.5°C/minute until it reached the target temperature. In the final stage, the sample was held isothermally at final temperature to achieve a total experiment duration of 2 hours. For the isothermal reduction experiments, the reduction was performed by introducing and held the sample isothermally at 1000°C, 1300°C, or 1450°C for 2 hours. Afterwards, the reduced briquette was mounted

for further examination using an optical microscope, ImageJ, and SEM-EDS.

Table 1. Chemical composition of natrojarosite (wt%).

SiO_2	Al_2O_3	$Fe_2O_{3(T)}$	MnO	MgO	CaO	Na_2O	K_2O	TiO_2
6.45	7.19	16.82	0.97	3.83	10.81	2.18	0.01	0.02

P_2O_5	Co_2O_3	Cr_2O_3	CuO	NiO	V_2O_5	ZnO	SO_3	LOI
0.02	0.06	0.23	0.01	1.34	0.01	0.03	13.92	36.09

Table 2. Chemical composition of natrojarosite (wt%).

SiO_2	Al_2O_3	$Fe_2O_{3(T)}$	MnO	MgO	CaO	Na_2O	K_2O	TiO_2
20.15	5.61	59.01	0.19	2.72	0.57	0.12	0.02	0.23

P_2O_5	Co_2O_3	Cr_2O_3	CuO	NiO	V_2O_5	ZnO	SO_3	LOI
0.01	0.06	3.46	0.01	0.58	0.04	0.03	1.27	5.94

Table 3. Proximate analysis of palm kernel shell as reductant.

Fixed Carbon	Volatile Matter	Ash	Inherent Moisture
18.60%	69.16%	2.88%	9.36%

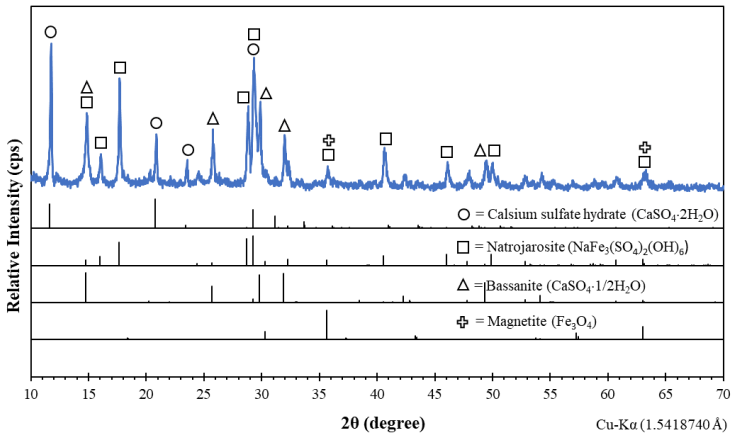

Fig. 1. XRD pattern of natrojarosite.

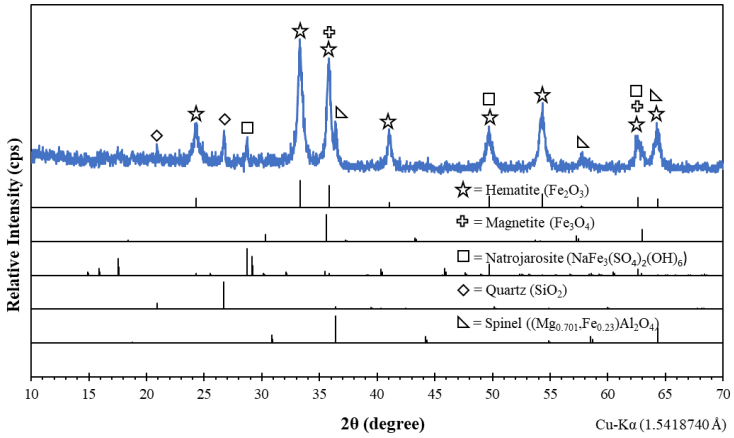

Fig. 2. XRD pattern of leaching residue.

3 Results and discussion

3.1 Effect of reductant amount and temperature on weight loss

Weight loss from the reduction process for the experiments with varying reductant amounts are presented in Figure 3. It can be observed that the weight loss of the reduced samples in the range of 25%-100% reductor exhibit a consistently increasing trend with the rise in the amount of reductant. The increase in weight loss is attributed to the increasingly reducing atmosphere within the system, wherein a greater quantity of metal oxides is converted to pure metal and gaseous products. Additionally, the removal of the volatile matter content of the palm kernel shell reductant also contributes to the overall weight loss. The volatile matter content within the sample increases with the increasing reductant amount, resulting in more volatile matter being evaporated and consequently leading to increasing sample weight change.

The physical appearances of the reduced samples for 25%, 50%, 75%, and 100% reductor variations are displayed in Figure 4 (a), (b), (c), and (d), respectively. For the 25% reductant addition, the reduced sample consists of concentrated metal and slag forming into granules with varying sizes. Whereas for higher amounts (≥50%) reductant addition, the reduction products remain in the form of un-sintered powder. The metals produced from experiments using 50%-100% reductor tend to be in microscale and are mixed with their respective slag. In the case of 25% reductant addition, the lower melting temperature of 1450°C causes the sample to undergo melting during reduction, leading to the separation of molten metal and slag based on their densities. On the other hand, for experiments with 50%-100% reductant addition, the excessive amount of reductor hinders contact between product particles, thus preventing significant agglomeration and leading to product having un-sintered appearance.

Figure 5 (a) and (b) show the influence of temperature on weight loss, both for non-isothermal and isothermal methods. Higher reduction temperatures create a more reducing atmosphere, leading to an increasing degree of reduction, as evidence by the greater weight loss at higher reduction temperatures.

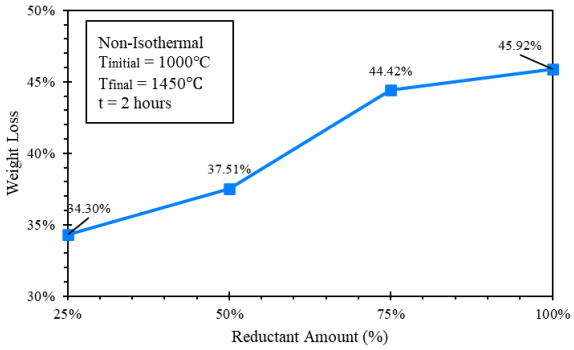

Fig. 3. Effect of reductant amount on weight loss for samples from non-isothermal reduction method at final temperature of 1450°C.

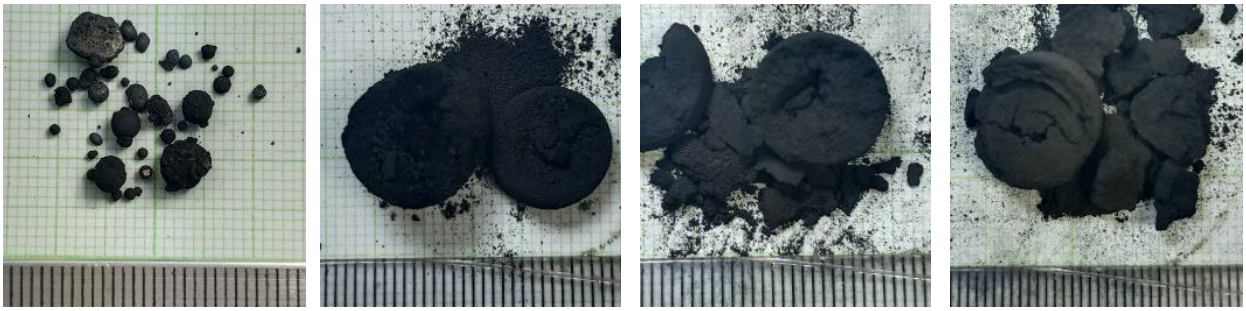

(a) (b) (c) (d)

Fig. 4. Physical appearance of non-isothermal reduction samples (T_{final} = 1450°C) using reductant amount of (a) 25%, (b) 50%, (c) 75%, and (d) 100%.

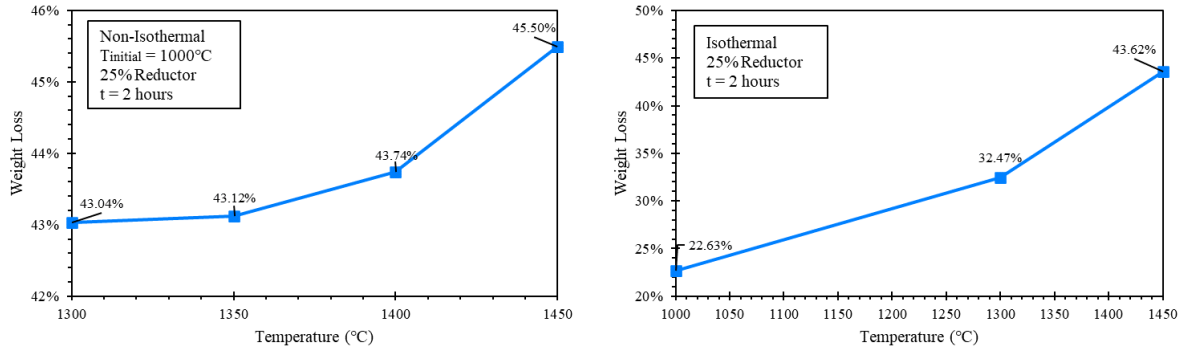

(a) (b)

Fig. 5. Effect of temperature on weight loss for samples with 25% reductant addition for (a) non-isothermal and (b) isothermal reduction method.

3.2 Effect of temperature on metal, matte, and slag composition

The quantitative analysis of the metal phase in the reduced samples is shown in Figure 6(a). The result indicates that increasing the temperature leads to a decrease in the Fe content in the metal phase. This occurs because other metal oxides, such as Cr_2O_3 and NiO, are also reduced, resulting in a lower Fe content in the metal phase. Higher temperatures create a more reducing atmosphere, leading to an increase in the degree of reduction. This is demonstrated by the increased amount of SiO_2 being reduced to Si and dissolving into the metal phase. Whilst the sulfur trend tends to decrease in the metal phase as the temperature increases, as sulfur tends to concentrate more in the matte phase at higher temperatures.

For the matte phase, the Fe trend is similar to that in the metal phase, showing a decrease in Fe content at higher temperatures due to the reduction of other oxide compounds, such as Si, Mn, and Cr, as shown in Figure 6(b). On the other hand, the sulfur content in the matte phase tends to increase steadily with increasing temperature.

The quantitative analysis of oxide compositions within the slag is shown in Figure 6(c). Increasing the temperature rises the compositions of CaO and Al_2O_3 in the slag while maintaining a constant MgO content. The trend of FeO content in the slag decreases with increasing temperature until 1400°C and then increases drastically at 1450°C. This increase in FeO content possibly occurs due to unwanted side reactions between the sample and the remaining air in the muffle furnace, which is difficult to eliminate.

On the other hand, higher temperatures can reduce the SiO_2 content in the slag. At 1300°C, the SiO_2 content is 60.49%, which then decreases to 48.15% at 1450°C. The increase in temperature leads to increasing reduction of SiO_2 to Si which then dissolves into the metal or matte phases. The reduction condition, however, was not sufficiently reducing for CaO, MgO, and Al_2O_3 since these components are stable in their oxide forms as indicated by their highly negative Gibbs Free Energy formation values.

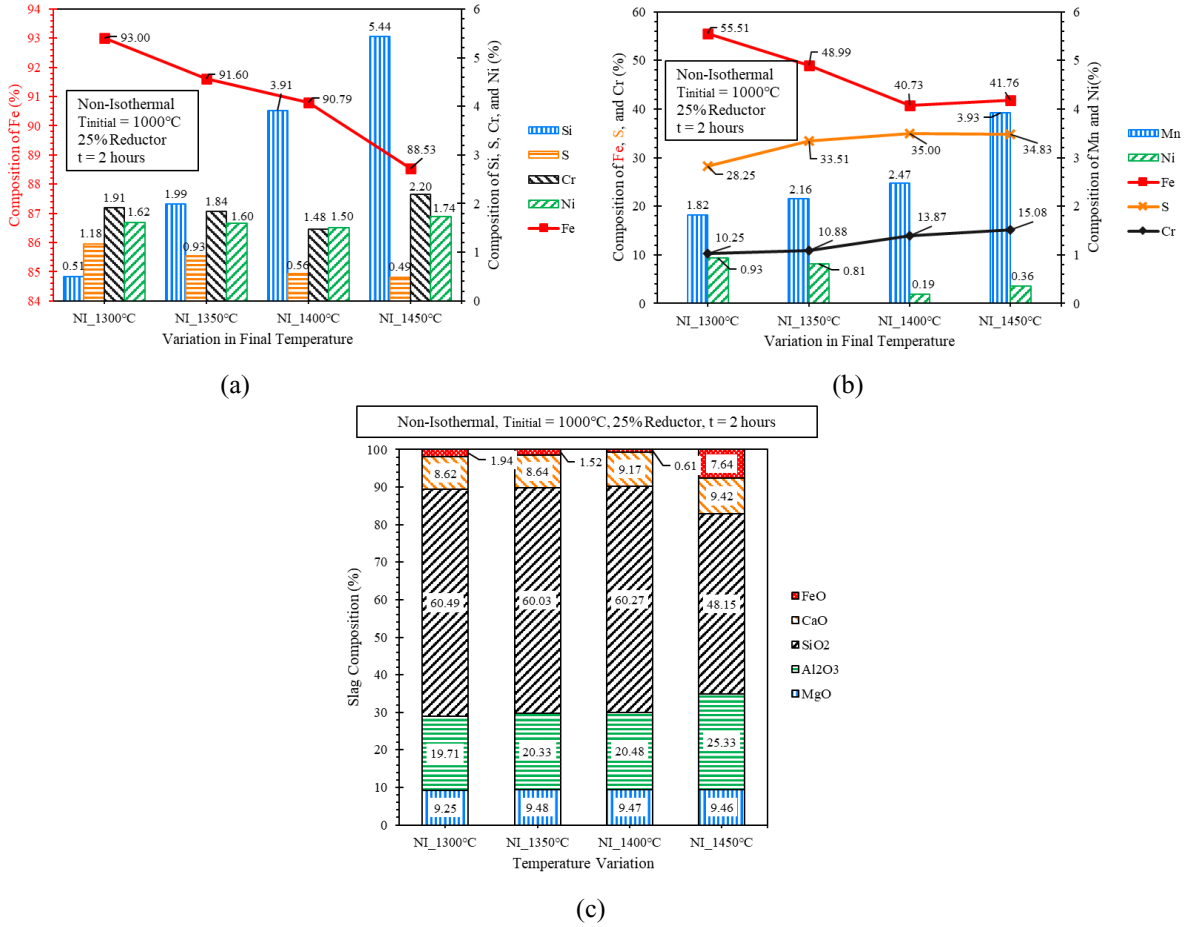

Fig. 6. Chemical composition of (a) metal phase, (b) matte phase, and (c) slag phase from non-isothermal reduction experiments.

The quantitative analysis of the metal phase from the isothermal temperature experiment is presented in Figure 7(a). Increasing the temperature results in an increase in the Fe and Ni contents. The Fe content increases significantly from 41.02% at 1000°C to 96.41% at 1300°C. Further increase in temperature does not significantly impact the Fe content in the metal phase. Si and Cr show a similar trend where they decrease from 1000°C to 1300°C and then increase at 1450°C. Sulfur in the metal phase exhibits the highest content at the reduction temperature of 1000°C. At this temperature, a complete separation between the metal and matte phases has not occurred due to the temperature not being high enough for diffusion to facilitate agglomeration of the metal and matte phases.

The trends in elemental content in the matte phase from isothermal reduction are shown in Figure 7(b). Increasing the temperature from 1000°C to 1450°C reduces the Fe content in the matte from 80.80% to 61.48%. This decrease in Fe content is due to more Mn, Ni, and Cr being dissolved into the matte solution phase. As the temperature increases to 1450°C, the oxide phases of Mn, Ni, and Cr are converted to sulfide solution which is evident from their increasing contents in the matte phase.

The composition of the slag from isothermal reduction shows a fluctuating trend at the three reduction temperatures, as shown in Figure 7(c). Increasing the temperature from 1000°C to 1300°C increases the MgO, Al_2O_3, and SiO_2 content in the slag. This increase occurs because a significant portion of FeO in the slag (which has a substantial content at 1000°C) is reduced to form its metal. Furthermore, at higher temperatures up to 1450°C, the MgO, Al_2O_3, and FeO content increases, while the SiO_2 content decreases from 57.01% to 35.86%. The decrease in SiO_2 content in the slag indicates a highly reducing atmosphere within the system, which can reduce SiO_2 to form Si metal which is then dissolved into the metal phase.

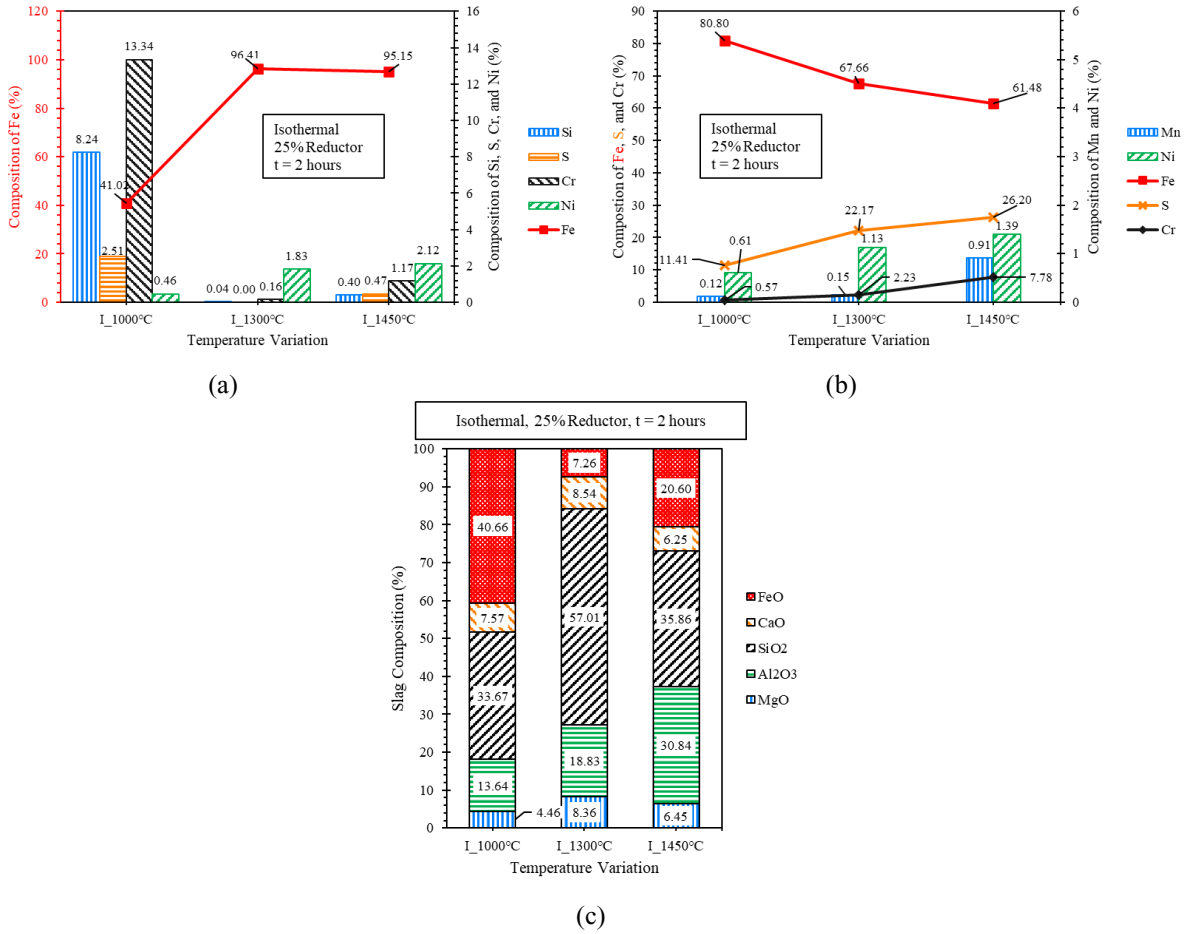

Fig. 7. Chemical composition of (a) metal phase, (b) matte phase, and (c) slag phase from isothermal reduction experiments.

3.3 Proportion of reduced phase

The equation used to determine the proportion of phase is given by Equation (1):

$$\text{Proportion of Phase X} = \frac{\text{Area of X} \times \text{Density of X}}{\sum \text{Area (X,Y,Z)} \times \text{Density (X,Y,Z)}} \times 100\% \quad (1)$$

Figure 8 shows the proportion of each phase for various temperature reduction profiles. As the reduction temperature increases from 1300°C to 1400°C in non-isothermal methods, the proportion of the metal phase increases, while the slag phase decreases. The increase in the proportion of the metal phase is due to the higher reduction temperature creating a more reducing atmosphere, facilitating the reduction of metal oxides in the slag into their metallic phases. Additionally, at higher temperatures, the separation process between metal and slag occurs more easily, resulting in better separation of metals that could potentially be trapped within the slag phase.

A similar trend is observed in the isothermal reduction method, which represents equilibrium conditions of the reduction process at temperatures of 1000°C, 1300°C, and 1450°C. At 1000°C, only a small amount of metal oxide is reduced to metal. The reduced phases are still predominantly in the form of oxides, and the resulting metals are relatively microscale (with size below 0.35 mm). As the reduction temperature is raised, microscale metals tend to combine and form larger iron granules (with size above 0.35 mm). The highest proportion of the metal phase is obtained at a reduction temperature of 1450°C, where the metals have combined to form one dominant large iron metal phase in the reduced samples.

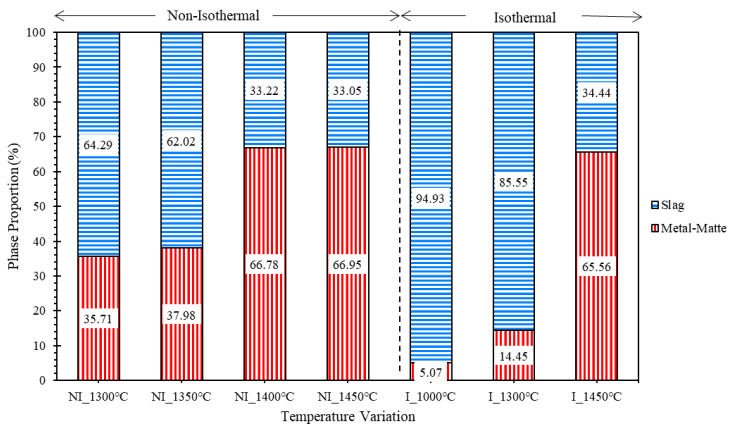

Fig. 8. Proportion of the reduced phase for various reduction temperature profiles

3.4 Reduced phase analysis

Figures 9 (a), (b), and (c) and Table 4 show the phase identification of the reduced samples. In the isothermal reduction at 1000°C, the formed phases are $CaAl_2Si_2O_8$, $CaMg_2Al_{16}O_{27}$, Fayalite (Fe_2SiO_4), and FeO in equilibrium with metallic Fe and FeS in matte. When the temperature is raised to 1300°C, the fayalite present in the slag from the 1000°C reduction undergoes decomposition. As a result, some Fe and Si within the slag migrate towards the metallic phase, leading to a composition dominated by liquid slag and cordierite ($Al_4Mg_2Si_5O_{18}$). Further increase in reduction temperature to 1450°C causes the briquetted sample to melt more easily, leading to a clearer separation between the metal, matte, and slag phases. Chromium (Cr), which was initially associated with the slag as Cr_2O_3, releases its oxygen bonds and forms CrS by reacting with sulfur towards the matte phase. The phase change from Cr_2O_3 to CrS occurs because the Gibbs free energy of CrS formation at high temperatures is more negative than that of Cr_2O_3 formation thermodynamically. Additionally, the phase analysis shows that liquid slag is the predominant oxide phase which indicates that the liquidus point of the slag has been surpassed.

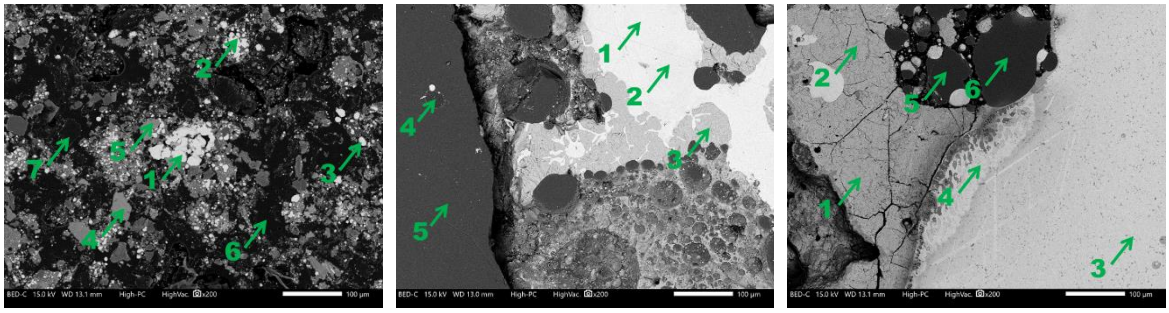

(a) (b) (c)

Fig. 9. Microstructures of the reduced products from (a) isothermal reduction at temperature of 1000°C, (b) non-isothermal reduction at final temperature of 1300°C, and (c) non-isothermal reduction at final temperature of 1450°C.

Table 4. Phase and chemical composition analysis of the reduction product from experiments at various reduction temperature profiles.

Reduction Condition			No	Composition (wt%)									Phases
Method	T (°C)	Reductant Amount		O	Na	Mg	Al	Si	S	Ca	Cr	Fe	
Isothermal	1000	25%	1	4.30	0.00	0.05	0.14	1.35	11.41	0.12	0.57	80.80	Metal
			2	33.44	0.01	3.50	9.26	16.80	0.00	11.80	2.60	20.06	$CaAl_2Si_2O_8$ & FeO
			3	22.34	1.24	3.74	7.73	25.24	4.25	3.57	2.04	24.88	$CaMg_2Al_{16}O_{27}$ & FeO
			4	22.77	1.07	3.05	6.98	12.35	3.28	2.39	2.09	43.83	Olivine: Fayalite
			5	13.55	0.57	1.40	9.90	4.12	1.74	1.24	24.59	38.20	Olivine: Fayalite
			6	59.30	0.00	0.43	3.61	6.29	0.00	0.70	0.16	28.43	FeO
			7	45.32	2.66	0.89	2.35	1.73	11.51	1.13	1.10	27.16	FeO
		25%	1	0.82	0.00	0.07	0.12	0.45	1.07	0.00	1.96	93.27	Metal

Non-Isothermal	1000 to 1300		2	1.36	0.00	0.06	0.02	0.56	1.28	0.01	1.86	92.73	Metal
			3	2.35	0.00	0.14	0.07	0.21	28.25	0.08	10.25	55.51	Matte
			4	44.83	1.48	5.55	10.38	28.14	0.00	6.13	0.43	1.50	Cordierite ($Al_4Mg_2Si_5O_{18}$)
			5	46.88	1.41	5.77	10.28	28.36	0.00	4.92	0.43	0.38	Slag-liq
Non-Isothermal	1000 to 1450	25%	1	1.19	0.00	0.10	0.08	5.45	0.63	0.02	2.14	88.35	Metal
			2	1.18	0.00	0.08	0.04	5.42	0.35	0.01	2.25	88.71	Metal
			3	1.16	0.05	0.12	0.10	5.45	1.10	0.00	2.51	87.63	Metal
			4	3.76	0.04	0.16	0.07	5.72	0.71	0.06	1.86	85.34	Metal
			5	2.11	0.12	0.43	0.07	0.27	34.24	0.43	15.08	42.30	Matte
			6	1.20	0.15	0.65	0.06	0.18	35.41	0.88	15.08	41.21	Matte
			7	35.13	1.04	5.75	13.45	22.17	4.20	6.61	1.02	8.85	Slag-liq
			8	36.77	1.06	6.18	14.57	24.88	3.37	7.46	0.56	3.57	Slag-liq

The results of ternary diagram simulations are presented in Figure 10 for slag from non-isothermal reduction experiment and in Figures 11, 12, and 13 for slag from isothermal reduction experiments. The summary of dominant phases, melting temperatures, and viscosities of the slag is provided in Table 5.

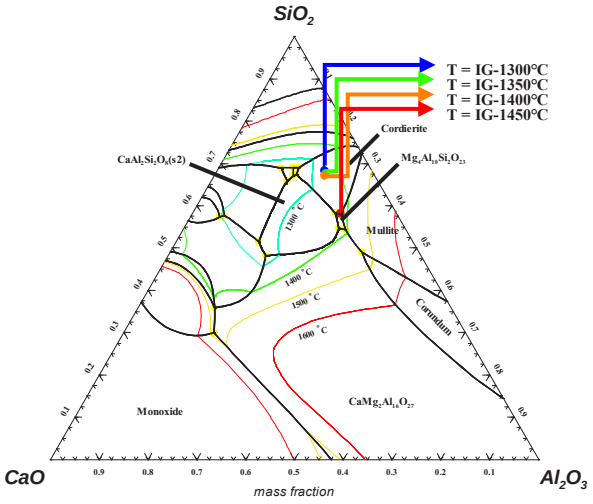

Fig. 10. Ternary diagram of SiO_2 – CaO – Al_2O_3 – MgO – FeO – Fe system for a(Fe(s)) = 1, MgO/Z = 0.0941, FeO/Z = 0.0293 where Z = (SiO_2 + CaO + Al_2O_3 + MgO + FeO) at 1 atm.

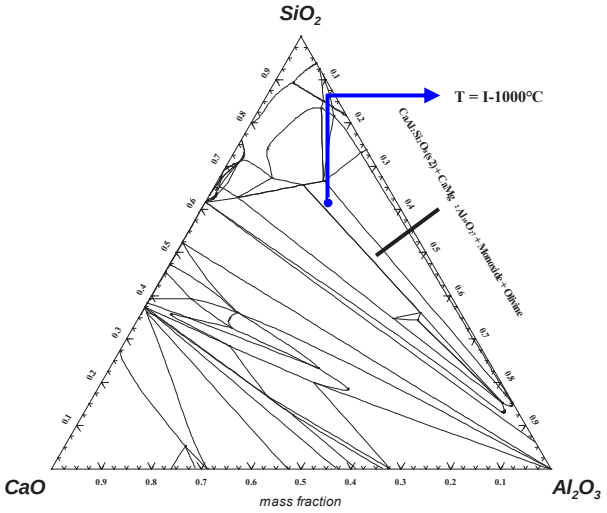

Fig. 11. Ternary diagram of SiO_2 – CaO – Al_2O_3 – MgO – FeO – Fe system for a(Fe(s)) = 1, MgO/Z = 0.0642, FeO/Z = 0.4066 where Z = (SiO_2 + CaO + Al_2O_3 + MgO + FeO) at T = 1000°C and P = 1 atm.

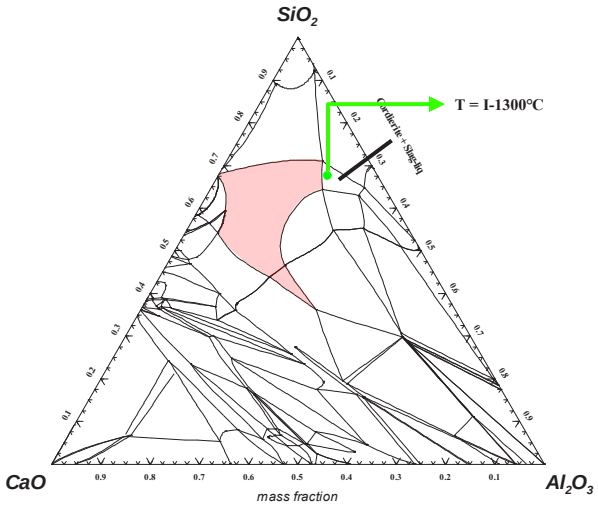

Fig. 12. Ternary diagram of SiO_2 – CaO – Al_2O_3 – MgO – FeO – Fe system for a(Fe(s)) = 1, MgO/Z = 0.0642, FeO/Z = 0.0726 where Z = (SiO_2 + CaO + Al_2O_3 + MgO + FeO) at T = 1300°C and P = 1 atm.

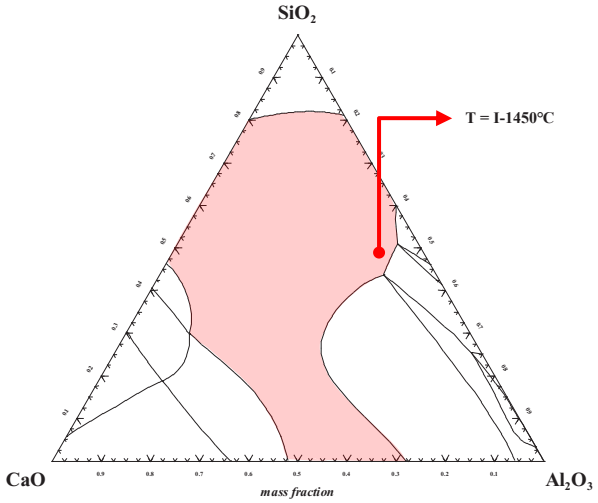

Fig. 13. Ternary diagram of SiO_2 – CaO – Al_2O_3 – MgO – FeO – Fe system for a(Fe(s)) = 1, MgO/Z = 0.0642, FeO/Z = 0.2060 where Z = (SiO_2 + CaO + Al_2O_3 + MgO + FeO) at T = 1450°C and P = 1 atm.

Table 5. Dominant phases, melting point, and viscosity of slag in the reduced sample

No	Conditions	Dominant Phases	Melting Point	Viscosity (PaS)
1	Non-Isothermal, 1300°C	Cordierite ($(Mg,Fe)_2Al_4Si_5O_{18}$)	< 1400°C	446.340
2	Non-Isothermal, 1350°C	Cordierite ($(Mg,Fe)_2Al_4Si_5O_{18}$)	< 1400°C	191.776
3	Non-Isothermal, 1400°C	Cordierite ($(Mg,Fe)_2Al_4Si_5O_{18}$)	< 1400°C	100.152
4	Non-Isothermal, 1450°C	Cordierite ($(Mg,Fe)_2Al_4Si_5O_{18}$) Slag-liquid	< 1400°C	7.313
5	Isothermal, 1000°C	$CaAl_2Si_2O_8$, $CaMg_2Al_{16}O_{27}$, Monoxide (FeO), Olivine ($(Mg,Fe)_2SiO_4$)	< 1400°C	8.625
6	Isothermal, 1300°C	Cordierite ($(Mg,Fe)_2Al_4Si_5O_{18}$) Slag-liquid	< 1400°C	140.569
7	Isothermal, 1450°C	Slag-liquid	< 1400°C	1.368

The non-isothermal reduction method has a melting point below 1400°C, meaning that as the reduction temperature increases, the slag becomes more prone to melting, facilitating the separation process between metal and slag. The dominant phase for the slag at temperatures between 1300°C and 1400°C is cordierite, while at 1450°C, it is dominated by liquid slag due to the melting temperature being surpassed by the experimental temperature. The shift in the equilibrium points on the ternary diagram at 1450°C is a result of the high content of FeO and Al_2O_3 within the slag.

Dominant phases at the thermodynamic equilibrium of reduction can be explained using the data from the isothermal reduction slag after 2 hours reduction process. Initially, at 1000°C, there are four phases in the slag, namely $CaAl_2Si_2O_8$, $CaMg_2Al_{16}O_{27}$, Monoxide

(FeO), and Olivine ($(Mg,Fe)_2SiO_4$). As the reduction temperature increases, some FeO and SiO_2 within the slag are reduced, leading to a phase change into Cordierite ($(Mg,Fe)_2Al_4Si_5O_{18}$) at 1300℃ and liquid slag at 1450℃ due to the liquidus temperature of the slag being exceeded.

The viscosity of the reduced slag is dependent on its composition and reduction temperature. The experimental results show a decreasing trend in viscosity with increasing temperature, which is in line with the Arrhenius' basic viscosity equation stated in Equation (2)[12]:

$$\eta = A \times \exp\left(\frac{E}{RT}\right) \quad (2)$$

where:
η = Viscosity
A = Arrhenius constant
E = Activation energy
R = Ideal Gas Constant
T = Temperature

However, the deviations in viscosity that occur at the isothermal reduction temperature of 1000℃ may be due to the briquetted sample inside the furnace not being fully reduced (still in powder form) and not entirely melted yet.

4 CONCLUSION

1. Increasing the amount of reductor and temperature may increase the weight loss of reduced sample. Iron with size more than 0.35 mm was only observed at 25% reductant addition for temperatures range of 1300-1450℃.
2. The higher the reduction temperature, the fewer iron present in the metal phase due to Cr and Ni derived from their oxides. Furthermore, at higher temperature, some SiO_2 is also reduced to the metal phase so the proportion of SiO_2 in the slag will decrease. Increasing the temperature helps to reduce the sulfur concentration in the metal phase which then accumulate in the matte phase.
3. The proportion of metal-matte increases with increasing temperature and the highest value obtained is at 1450℃ non-isothermal reduction of 66.95%.
4. The best slag characteristics are achieved at 1450℃ non-isothermal reduction because it has a low viscosity, 7.313 PaS, with the main phases of liquid slag and low fraction of FeO in slag, namely 7.64%.

Acknowledgements

This research was funded by Ministry of Education, Culture, Research, and Technology of the Republic of Indonesia, 2023 (No. 007/E5/PG.02.00.PL/2023). The authors thanks to PT Hydrotech Metal Indonesia and PT Perkebunan Nusantara VIII who provided samples for this study. The authors would like to acknowledge the support from PT Gunbuster Nickel Industry for providing the Scanning Electron Microscope-Energy Dispersive X-ray Spectroscopy JEOL JCM-7000 NeoScopeTM used for the analysis of the samples in this work. The authors would also like to acknowledge the support from the Department of Mineral Sciences of the Smithsonian Institution for providing Basaltic Glass and Springwater Olivine reference materials.

References

1. U. G. Survey, "Mineral Comodity Summaries", (2022).
2. P. Prasetyo, IOP Conf. Ser.: Mater. Sci. Eng. **285**, 012015 (2018)
3. Staltechnology.com (2020)
4. X. Min, X. Xie, L. Chai, Y. Liang, M. Li, and Y. Ke, Transactions of Nonferrous Metals Society of China **23**, 208 (2013)
5. D. M. Franks, D. V. Boger, C. M. Côte, and D. R. Mulligan, Resources Policy **36**, 114 (2011)
6. W. Ma, D. Schott, and G. Lodewijks, Minerals **7**, 47 (2017)
7. D. Zhu, Journal of Cleaner Production 8 (2018)
8. T. Gultom and A. Sianipar, IOP Conf. Ser.: Earth Environ. Sci. **413**, 012015 (2020)
9. C. A. Ang, F. Zhang, and G. Azimi, ACS Sustainable Chem. Eng. **5**, 8416 (2017)
10. D. Gwyther, Marine Pollution Bulletin **48**, 997 (2004)
11. A. Özverdİ and M. Erdem, Hydrometallurgy **100**, 103 (2010)
12. L. Darabi and M. Zare, Chemical Physics **539**, 110933 (2020)